Anthropogenic intensification of surface ocean interannual pCO_2 variability

M. Angeles Gallego[1], Axel Timmermann[2,3], Tobias Friedrich[1], and Richard E. Zeebe[1]

[1]Department of Oceanography, School of Ocean and Earth Sciences and Technology, University of Hawaii at Manoa, Honolulu, Hawaii, USA
[2]Center for Climate Physics, Institute for Basic Science (IBS), Busan, South Korea
[3]Pusan National University, Busan, South Korea

Key Points:

- The interannual oceanic pCO_2 variability is amplified by the end of 21st century in most of the world's oceans.
- The amplification in pCO_2 variability is due to an increased oceanic sensitivity to dissolved inorganic carbon and temperature variations.
- A decrease of the dissolved inorganic carbon fluctuations counteracts the amplification, but the models differ in this projection.

Corresponding author: M. Angeles Gallego, mdla@hawaii.edu

This article has been accepted for publication and undergone full peer review but has not been through the copyediting, typesetting, pagination and proofreading process which may lead to differences between this version and the Version of Record. Please cite this article as doi: 10.1029/2020GL087104

©2020 American Geophysical Union. All rights reserved.

Abstract

We use several global coupled atmosphere-ocean-biogeochemistry models from the Coupled Model Intercomparison Project (CMIP5), to show that the global interannual variability of the sea-surface pCO_2 (calculated as 1σ) will increase by $\sim 64 \pm 20\%$ by 2040-2090 relative to the beginning of the industrial revolution under the RCP8.5 scenario. All models agree that the increase in variability is a consequence of a larger background pCO_2 and a lower buffering capacity that enhance the response of pCO_2 to the fluctuations of surface temperature (T) and dissolved inorganic carbon (DIC). The most skillful group of models under present-day conditions shows a future global decrease in DIC fluctuations that will weaken the pCO_2 interannual variability (IAV). The remaining uncertainties in the projected evolution of pCO_2 variability regionally highlight the need for continuous carbon monitoring programs which will contribute to a better understanding of the oceanic carbon sink's response to increased green house emissions.

Plain Language Summary

We used a series of coupled climate/carbon cycle models to show that the year-to-year variations in the oceanic surface partial pressure of carbon dioxide, will intensify by the end of the 21st century. The future interannual fluctuations in carbonate chemistry will have a stronger impact on surface ocean pCO_2, because anthropogenic carbon emissions make the ocean less able to buffer these natural changes. Earth system models also document and overall weakening of the underlying biophysical interannual changes, which can partly compensate for the enhancement of pCO_2 in some areas, such as the eastern equatorial Pacific. Projected changes in the ocean's carbon dioxide levels will also impact the flux of carbon between the atmosphere and the ocean, and therefore, play an important role in the uptake of anthropogenic carbon and the level of future greenhouse warming.

1 Introduction

On average, the ocean absorbs 2.4 ± 0.5 Pg of carbon each year (Le Quéré et al., 2018) but the efficiency of the oceanic carbon sink varies on interannual time-scales. Efforts have been made to estimate the present-day year-to-year variations of CO_2 uptake in observations and models (Dong et al., 2017), however there is little agreement. Moreover, numerous studies use different variability metrics which makes it difficult to compare the estimates. Values for the interannual variability calculated as 1 σ of the CO_2 flux anomalies range from ± 0.14 PgC yr^{-1} for a 1982-2007 diagnostic model (Park et al., 2010), ± 0.29 for the 1985-2017 observations (Le Quéré et al., 2018), $\pm$ 0.31 PgC yr^{-1} for a 1992-2009 data-based estimation (Rödenbeck et al., 2015) to ± 0.40 PgC yr^{-1} for a 1979-1997 simulation (Le Quéré et al., 2000).

The ocean-atmosphere flux of CO_2 (FCO_2) is determined by the difference between ocean and atmospheric pCO_2, and further modulated by solubility, regional wind speed and sea ice coverage. Globally, most of the open ocean's FCO_2 interannual variability is driven by the fluctuations in oceanic pCO_2 (Landschützer et al., 2016; Landschützer, Ilyina, & Lovenduski, 2019; Rödenbeck et al., 2015; Li et al., 2019), however in some regions wind speed variations can also have an important impact (Doney et al., 2009; Wanninkhof & Triñanes, 2017).

The ocean's pCO_2 interannual variability (from now on referred as IAV) is generated by large scale atmosphere-ocean interactions and specific climate modes, such as the El Niño Southern Oscillation (ENSO) in the equatorial Pacific, the Pacific Decadal Oscillation (PDO) in the North Pacific, the Southern Annular Mode (SAM) in the Southern Ocean, and the North Atlantic Oscillation (NAO). These climatic phenomena induce

©2020 American Geophysical Union. All rights reserved.

changes in physical parameters (e.g. temperature, salinity, ocean currents, mixing) which in turn influence ocean biology and carbonate chemistry, thereby altering the ocean's ability to sequester CO_2 (Doney et al., 2009; Feely et al., 2002; Chatterjee et al., 2017; Sutton et al., 2017; McKinley et al., 2004; Friedrich et al., 2006; Landschützer, Ilyina, & Lovenduski, 2019).

The oceanic pCO_2 is completely determined by dissolved inorganic carbon (DIC), total alkalinity (TA), temperature (T) and salinity (S). The interannual climate modes of variability alter the DIC, TA, T and S, but the impact of these anomalies on the pCO_2 depends on the sensitivity of the seawater's carbonate chemistry. In the ocean, approximately 89% of the dissolved inorganic carbon occurs in the form of bicarbonate (HCO_3^-) and $\approx$ 10.5% as carbonate (CO_3^{-2}); the CO_2 concentration ([CO_2]) only comprises a $\approx$0.5% (Zeebe & Wolf-Gladrow, 2001). The carbonate chemistry dynamics and the sensitivity of pCO_2 to changes in DIC, TA, T and S are strongly controlled by ambient CO_2. As the ocean captures CO_2, its ability to convert it into HCO_3^- and CO_3^{-2} decreases, and the pCO_2 sensitivity to any change in DIC increases. In the same way, a larger background aqueous [CO_2] enhances the effect of temperature on pCO_2's solubility.

The on-going decline on the ocean's buffering capacity due to increasing atmospheric CO_2 concentrations is well documented in the literature (Bates et al., 2014; Fassbender et al., 2017; Sabine et al., 2004; Egleston et al., 2010), and recently, the corresponding implications for the seasonal cycle amplitude of pCO_2 have been elucidated. To determine the effect of anthropogenic CO_2 on the seasonal cycle of the ocean's pCO_2 it is necessary to distinguish the influences of carbonate chemistry dynamics from those directly related to biophysical mechanisms. This can been done using a Taylor series expansion of pCO_2 in terms of the physical and chemical main drivers (McNeil & Sasse, 2016; Landschützer et al., 2018; Gallego et al., 2018; Fassbender et al., 2018) and through idealized simulations (Hauck & Völker, 2015; Gorgues et al., 2010). These studies concluded that the trends in carbonate chemistry are responsible for the increased seasonal amplitude of pCO_2 and hydrogen ion concentrations (Kwiatkowski & Orr, 2018). Yet, the impact of the decreasing ocean's buffering capacity on the interannual variability of pCO_2 has not been documented.

The large interannual variability induced by ocean-atmosphere interactions makes it difficult to detect long-term trends in the ocean's carbon sink (McKinley et al., 2017; Li et al., 2019; Chatterjee et al., 2017; Sutton et al., 2017), in particular on regional scales. However, some studies have shown that it is possible to use models and data-assimilation techniques to predict the carbon sink up to some extent (Séférian et al., 2018; Li et al., 2019). To further improve these predictions, we need to use carbon monitoring programs as well as mechanistic studies to understand the vulnerability of pCO_2 interannual variability to increasing greenhouse gas emissions (McKinley et al., 2017; Gruber et al., 2019).

Our aim in this study is to quantify how well CMIP5 models capture the mechanisms of present-day sea surface pCO_2 IAV when compared to data-based estimates, and from there, elucidate the causes of future changes in the variability of the carbon cycle in response to anthropogenic emissions of CO_2.

2 Methodology

Models

For our analysis, the surface pCO_2, DIC, TA, T and S monthly-mean output variables covering the period 1861-2005 were obtained from historical simulations, and the period 2006-2100 from climate change simulations forced with the Representative Concentration Pathway 8.5 (RCP8.5) greenhouse gas emission scenarios (IPCC, 2013). We selected 16 fully coupled earth system models that participated in the Coupled Model Intercomparison Project, Phase 5 (CMIP5) to analyze the standard deviation of pCO_2.

©2020 American Geophysical Union. All rights reserved.

Accepted Article

However, we removed from the analysis the models CMCC-CESM and GISS-E2-H-CC based on Dong et al. (2016) and the large difference between their patterns of pCO_2 standard deviation (STD) from those of other models and observations (see Supplement material S2, and the observation-based estimate of Figure 2). Out of the sixteen, we selected six models for a more comprehensive analysis of the causes driving pCO_2 variability; these models were selected based on data availability: CanESM2, CESM1-BGC, GFDL-ESM2G, MPI-ESM-LR, HadGEM2-ES and HadGEM2-CC (See supplementary material of Hauri et al. (2015)). The ocean's surface data sets were regrided onto a 1°x1° grid using Climate Data Operators (CDO). The Arctic Ocean and the region poleward of 70°S are removed from the analyses, because observational data for model validation are scarce.

Analysis

Commonly, the interannual anomalies are defined as deviations of monthly mean values from a long-term mean monthly climatology, or by using a running 12 month filter on detrended monthly values, (Landschützer, Ilyina, & Lovenduski, 2019; Rödenbeck et al., 2015). However, for CMIP5 models, the future seasonal cycle of pCO_2 is expected to increase (Gallego et al., 2018), therefore removing a mean climatology for the 1861-2100 period would result in an overestimation of IAV amplification (IAVA). On the other hand, a 12 month running filter would remove important sub-annual information associated with the coupling between the seasonal and interannual time-scales, such as Combination modes which play a key role for ENSO dynamics, (Stuecker et al., 2015). Finally, removing a linear trend from a 200-year-long time series poses its own difficulties. To avoid these issues, we calculate the monthly anomalies for each year as the monthly deviation from a 11-year running climatology centered on that year. For example, for the year 1935 we desasonalize the monthly values by subtracting the mean climatology from 1930 to 1940; for the year 1936 we use the climatology from 1931-1941 and so on. From now on, the monthly deviations (or anomalies) are denoted by pCO_2' and the running climatology as $\overline{pCO_2}$. Supplement Figure S1 shows the time series of $\overline{pCO_2}$ and pCO_2' obtained with this method. The size of the running window is arbitrary but is chosen to minimize the loss of data points at the end of the time series. We compared windows of 11, 21 and 31 years and the values for the mean $\overline{pCO_2}$ and the STD of pCO_2' are similar (see Supplement Figure S2).

To elucidate the underlying physical and chemical processes controlling the pCO_2 interannual anomalies (from now pCO_2') we calculated a first-order Taylor series expansion of pCO_2' in terms of its four controlling factors, DIC, TA, T and S, following the method of Takahashi et al. (1993); Lovenduski et al. (2007); Doney et al. (2009).

To remove the fresh water concentration/dilution effect we use salinity-normalized DIC and TA using a mean salinity of 35 psu, referred as DIC_s and TA_s, (Lovenduski et al., 2007). The freshwater effect is now included in the S_{fw} term. For the Taylor series expansion, each variable (X = DIC_s , TA_s , T and S_{fw}) is decomposed as $X = \overline{X} + X'$. The term $\overline{X}$ represents the mean climatology calculated for an 11-year running window at each grid point. The term X' are the monthly anomalies, calculated as the deviation from the mean climatology. The full first-order series expansion is given by:

$$pCO_2{}' \approx \frac{\partial pCO_2}{\partial DIC}\bigg|_{\overline{TA},\overline{DIC}\atop \overline{T},\overline{S}} DIC_s{}' + \frac{\partial pCO_2}{\partial TA}\bigg|_{\overline{TA},\overline{DIC}\atop \overline{T},\overline{S}} TA_s{}' + \frac{\partial pCO_2}{\partial T}\bigg|_{\overline{TA},\overline{DIC}\atop \overline{T},\overline{S}} T' + \frac{\partial pCO_2}{\partial S}\bigg|_{\overline{TA},\overline{DIC}\atop \overline{T},\overline{S}} S'_{fw}, \tag{1}$$

where the derivatives are evaluated on the running climatologies. The analytical derivation of Eq. (1) is given in the Supplementary material. Equation (1) can be rewritten as:

©2020 American Geophysical Union. All rights reserved.

Accepted Article

$$pCO_2{}' \approx \overline{pCO}_2 \cdot \left(\gamma_{DIC_s} \cdot DIC_s{}' + \gamma_{TA_s} \cdot TA_s{}' + \gamma_T \cdot T' + \gamma_S \cdot S_{fw}{}'\right) \quad (2)$$

where, for notation purposes, each derivative is re-defined as: $\gamma_{\mathrm{X}} = \frac{1}{\mathrm{pCO_2}} \cdot \frac{\partial \mathrm{pCO2}}{\partial \mathrm{X}}$, and we will refer to them as the *pCO_2 sensitivity to X*. It is important to make the distinction between different quantities that measure the oceanic buffering capacity. The DIC sensitivity (γ_{DIC}) is a similar concept to the Revelle factor (RF), and they are related by $\mathrm{RF} = \frac{\gamma_{\mathrm{DIC}}}{\mathrm{DIC}}$. Our definition of γ_{DIC} is the inverse of the one given by Egleston et al. (2010). The three different quantities RF, γ_{DIC} and $1/\gamma_{\mathrm{DIC}}$ characterize how much the $\mathrm{pCO_2}$ changes by a given change in DIC, but they differ in their spatial distribution in the oceans.

In what follows, we use the method of Doney et al. (2009) to determine how much each term (from DIC, TA, T and S) contributes to the variability of $\mathrm{pCO_2}$ (measured as the root-mean-square (RMS) of $\mathrm{pCO_2'}$). First, Equation (2) is multiplied by $\mathrm{pCO_2}'$, and then averaged, obtaining the following equation:

$$\begin{aligned} <(pCO_2{}')^2> \;\approx\; & \overline{pCO}_2 \cdot \gamma_{DIC_s} <DIC_s{}' \cdot pCO_2'> \;+\; \overline{pCO}_2 \cdot \gamma_{TA_s} <TA_s{}' \cdot pCO_2'> \\ & +\; \overline{pCO}_2 \cdot \gamma_T \;<T' \cdot pCO_2'> \;+\; \overline{pCO}_2 \cdot \gamma_S <S_{fw}{}' \cdot pCO_2'>, \end{aligned} \quad (3)$$

where $< ... >$ represents a temporal averaging operator. Introducing the following notation:

$$\beta_X \equiv \frac{<\overline{pCO}_2 \cdot \gamma_X \cdot X' pCO_2{}'>}{<(pCO_2')^2>}. \quad (4)$$

Then, we can divide Eq. (3) by $<(pCO_2')^2>$ to give the relationship $\sum_{\mathrm{X}} \beta_{\mathrm{X}} \approx 1$, where $\mathrm{X} = \{\mathrm{DIC}, \mathrm{TA}, \mathrm{T}, \mathrm{S}\}$, as introduced by Doney et al. (2009). Thus, if we multiply Eq.(4) by the RMS of the anomalies (defined as $\sqrt{<(pCO_2{}')^2>}$), then the β_X coefficients can be interpreted as the fraction of the total RMS of the $\mathrm{pCO_2'}$ that each variable contributes. In our numerical calculations the sum of the β's differs slightly from one due the approximation used for the Taylor expansion, and the anomalies averaged being slightly different from zero.

3 Results

The increase in IAV of surface $\mathrm{pCO_2}'$ is illustrated with the running standard deviation of the monthly anomalies from 1871 to 2090 (Figure 1). The ensemble mean (14 CMIP5 models) of the globally averaged STD of $\mathrm{pCO_2}$ increases from $7\pm 1.2\mu$atm to 11.8 ± 2.8 μatm by the end of the 21$^{\mathrm{st}}$ century. Detailed global maps for the periods 1866-1917 and 2045-2095 STD are found in Supplement material S2 and S3. For the $\mathrm{pCO_2}$, a present day comparison shows that the 1987-2012 ensemble STD is 8.6 μatm and is larger than the observation-based estimates of ≈ 4.4 μatm (Landschützer, Bushinsky, & Gray, 2019) (excluding the Arctic region).

The disagreement between models and the data-based results of Landschützer, Bushinsky, and Gray (2019) may be due to several reasons. First, the data-based estimations are an interpolation of the Surface Ocean $\mathrm{CO_2}$ Atlas (SOCAT) dataset (Bakker et al., 2016; Sabine et al., 2013) which may be biased due to under-sampling, and interpolation methods may cause a lower RMS in higher latitudes with limited observational coverage (Landschützer, Ilyina, & Lovenduski, 2019; Rödenbeck et al., 2015; Sutton et al.,

©2020 American Geophysical Union. All rights reserved.

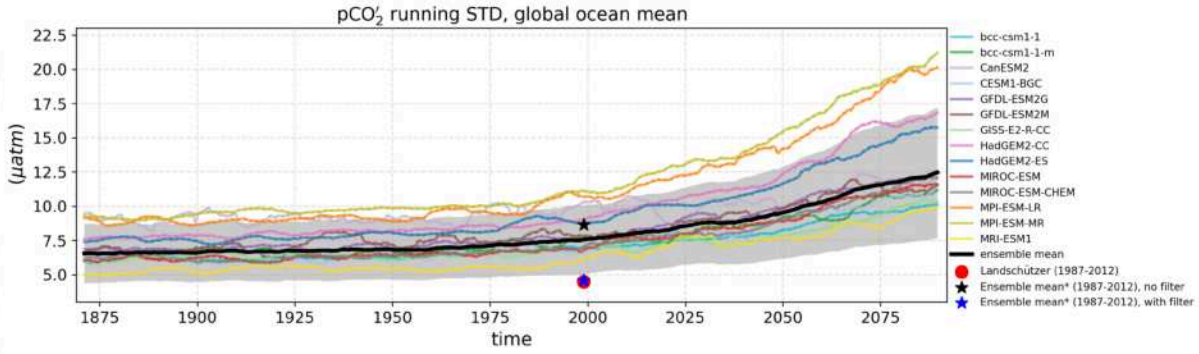

Figure 1. Increase in IAV of the sea surface pCO_2' as a function of time. The IAV is expressed as the running standard deviation (STD) of the monthly anomalies simulated for the historical and the high-emissions Representative Concentration Pathway 8.5 from 1861 to 2100. The STD is calculated using a 10 year moving window for each grid point and then globally averaged. The monthly anomalies for each year were calculated by removing a 11-year climatology centered around that year, in order to remove the positive trend and the increasing seasonal cycle amplitude. The final STD time series comprises the 1871-2090 period. Solid black line indicates the ensemble mean of the individual STDs; the grey area, $\pm 1\sigma$. The figure also shows the ensemble mean STD for the 1987-2012 period; for the unfiltered anomalies (black star), for the anomalies filtered with a 12-month running average (blue star) and for the unfiltered anomalies' of Landschützer, Bushinsky, and Gray (2019) dataset (red circle). The models CMCC-CESM and GISS-E2-H-CC were removed (see Methodology section).

2017, 2014). In another example of under-sampling related bias, it was found that the observed 1970-2011 pCO_2 anomalies show a larger standard deviation than the CIMP5 models, but they were of equal magnitude when the models were subsampled to the measurements, (Tjiputra et al., 2014). Secondly, it is important to notice that we use fully-coupled ocean-atmosphere models, therefore they generate their own internally driven climate variability and the amplitude and timing may not match with observational records. This is further analyzed in the next section. Third, the neural-network-based reconstruction approach used for the observations may smooth away important sub-annual variations (Gruber et al., 2019). To test this hypothesis, we apply a 12-month running mean to filter out sub-annual variability in the models' anomalies. When we apply the filter, we find a global mean STD of ≈ 4.5 μatm, very similar to the unfiltered anomalies of Landschützer, Bushinsky, and Gray (2019) (see Figure 1 and Supplement Material Figure S2 (b)). However, the sub-annual variations captured in the models are specially important in regions with high variability. In the Southern Ocean, the pCO_2 interannual variability is highly coupled to the seasonal cycle. Gregor et al. (2018) found that winter wind stress explains decadal variability and summer drivers explains interannual variability in this region. Moreover, Stuecker et al. (2015) suggests that ENSO should not be studied only on interannual time-scales, since is strongly coupled to the seasonal cycle which lead to the generation of variability on timescales of 9 and 15-18 months. Given on these considerations, we decided to conduct our study with unfiltered anomalies, recognizing that the background level of natural variability from this approach may differ from the observation-based reconstructions of Landschützer, Bushinsky, and Gray (2019).

©2020 American Geophysical Union. All rights reserved.

Accepted Article

Drivers of present-day sea surface pCO_2 interannual variability

The drivers of the present-day (1987-2010) pCO_2' interannual variability are analyzed in Figure 2. We compare the root mean square (RMS) of simulated pCO_2' and the respective contributions of T, DIC,TA and S for the 1987-2010 period with the reconstruction of Landschützer, Bushinsky, and Gray (2019). For the observation-based dataset we only calculate the thermal and non-thermal components using observed sea-surface temperatures (TA and DIC are not available). The non-thermal component comprises the combined contribution of DIC, TA and S, (Takahashi et al., 2002). The thermal and non-thermal contributions calculated for the CMIP5 models can be found in Supplement material (Figure S4); these follow the DIC and T patterns respectively.

The spatiotemporal-patterns and drivers of the present-day pCO_2's IAV have been largely documented in the literature and are well captured in the estimate of Landschützer, Bushinsky, and Gray (2019) shown in Figure (2) and further analyzed in Landschützer, Ilyina, and Lovenduski (2019) . Studies agree that most of the global pCO_2 IAV is generated in the equatorial Pacific (Doney et al., 2009; Rödenbeck et al., 2015; McKinley et al., 2017) and the equatorial belt may account for 40% of the total temporal standard deviation of the global Ocean, (Rödenbeck et al., 2014). Previous studies also agree that the pCO_2's IAV is controlled by non-thermal changes in the high latitudes (Resplandy et al., 2015; Verdy et al., 2007) and in the equatorial Pacific, where during El Niño years the reorganization of oceanic currents reduce the upwelling or DIC-rich waters causing negative pCO_2 anomalies (Feely et al., 2006; Valsala et al., 2014; Sutton et al., 2014; Cosca et al., 2003; Long et al., 2013; Feely et al., 1999). In contrast, in the subtropical gyres the variability is controlled by thermal changes (Doney et al., 2009; Landschützer, Ilyina, & Lovenduski, 2019; Rödenbeck et al., 2015).

Thus, for analysis purposes, we separate the models into two groups according to the following characteristics: 1) the location of the maximum pCO_2 variability and 2) the pattern of thermal and non-thermal dominance of the pCO_2 IAV. The models CanESM2, CESM1-BGC and GFDL-ESM2G (from now on referred to as Group I) show the largest pCO_2 variability in the equatorial Pacific and a DIC-dominance in the equatorial belt and the high latitudes. These models are in good agreement with the observational estimates (Figure 2, second row). The models HadGEM2-CC/ES and MPIESM-MR (from now on referred to as Group II) have an overall poorer performance compared to Group I. For Group II, the strongest fluctuations occur in the high latitudes, especially in the Southern Ocean and North Atlantic, and the pCO_2 IAV is dominated by temperature in the equatorial Pacific. However, this group agrees with observations on the DIC-dominance in the high latitudes (Figure 2, third row).

The low equatorial variability in the Group II models may be a consequence of the CO_2 flux variability that exhibits a much shorter period variation than ENSO time-scales, thus ENSO does not play a dominant role on the IAV (Dong et al., 2016). Jin et al. (2019) performed a similar analysis of the IAV drivers in the equatorial Pacific region. The authors found that for CanESM2, CESM1-BGC and GFDL-ESM2G (Group I) the pCO_2 anomalies caused by El Niño are negative due to a redistribution of oceanic currents and reduced upwelling of DIC-rich waters; while for MPI-ESM-lR and HadGEM-ES/CC (Group II) the pCO_2 anomalies are positive as a consequence of the anomalous eastward advection of warmer waters. Group II fails to represent the DIC dominance because of a underestimated reduction in upwelling during El Niño years and weak mean vertical gradients of DIC.

Some other interesting differences and similarities between the models and the observations-based estimate are worth mentioning. For example, in the equatorial Atlantic the HadGEM2-CC/ES and GFDL-ESM2G models (from Group II and Group I respectively) show a negative temperature contribution (Wang et al., 2015), disagreeing with the Landschützer, Ilyina, and Lovenduski (2019) estimate. In the sub-polar North Atlantic the observations

©2020 American Geophysical Union. All rights reserved.

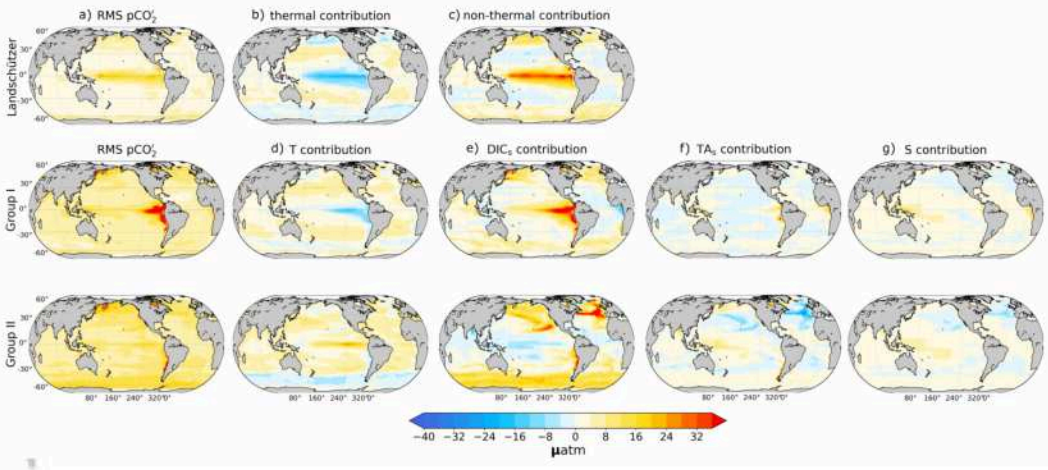

Figure 2. Mechanisms driving the 1987-2012 interannual variability of surface ocean pCO_2. First row shows the **a)** Landschützer, Bushinsky, and Gray (2019) estimate of the root mean square (RMS) of pCO_2 interannual anomalies, and its **b)** thermal and **c)** non-thermal contributions. The models were grouped according to their behavior (see main text) in Group I (CanESM2, CESM1-BGC and GFDL-ESM2G) and Group II (HadGEM2-CC, HadGEM-ES and MPI-ESM-LR) respectively. We first did an analysis of the RMS of the pCO_2' and its DIC, TA, T and S contributions for each individual model, and then we calculated the ensemble mean of Group I and Group II. The panels in the second and third rows show the ensemble mean of the Group I and II respectively, for the **a)** root mean square (RMS) of pCO_2 interannual anomalies and its contributions from **d)** temperature (T), **e)** dissolved inorganic carbon that has been salinity normalized (DIC_s), **f)** salinity normalized total alkalinity (TA_s) and **g)** salinity including fresh water effect (S_{fw}). For the observations, we calculate a thermal and non-thermal terms following Takahashi et al. (2002) method because there is not enough DIC, TA and S data available. The non-thermal component comprises the combined effects of DIC, TA and S. Following the method of Doney et al. (2009), each map of the contributions is calculated as the β coefficient of Eq. (4) normalized by the RMS of the pCO_2'. In the panels, yellow-redish colors indicate a positive contribution to the RMS of pCO_2 interannual anomalies and blue colors represent a negative contribution. Each model is depicted individually in the Supplement material Figure S5.

show a non-thermal dominance north of 40°N, whereas in the models the DIC dominance extends to 25-30 °N. Only the HadGEM2-CC/ES model shows a relatively important alkalinity contribution in the North Atlantic and North Pacific that counteracts the positive DIC contribution. Salinity has a minor effect everywhere, with a small positive effect in the western Pacific associated with rainfall changes due ENSO (see Supplement material Figure S5).

Future sea surface pCO_2 interannual variability

We further investigate the future spatio-temporal characteristics of the pCO_2 IAV. The sea surface pCO_2 IAV, calculated as the RMS-value of the interannual pCO_2 anomalies, is amplified in most of the ocean by the end of the 21^{st} century (Figure 3a), (see Supplement material Figure S5 for each individual model). Yet, the magnitude of the IAV amplification (IAVA) exhibits large regional differences, and even decreases in the

©2020 American Geophysical Union. All rights reserved.

equatorial Pacific for some models. Here, we analyze the causes of IAVA and its spatial heterogeneity by separating the analysis into the two groups of models mentioned in the previous section. For Group I the pCO_2 IAV increases everywhere except in the equatorial Pacific (see Figure 3a, upper row); Group II shows higher values of IAVA than Group I globally (see Figure 3a, bottom row).

To determine how much of the pCO_2 IAVA is due to carbonate chemistry dynamics and how much is explained by physical and biological processes, we calculate the RMS of $pCO_2{}'$ for the final period as if only the background carbonate chemistry - represented by $\overline{pCO_2}$ and the sensitivities (γ_T and γ_{DIC})- increase, but maintaining the historical values of the anomalies given by T′ and $DIC_s{}'$ (see Eq. (2)). The latter anomalies are the result of physical and biological variations. In both groups of models, the case in which only the carbonate chemistry is changed shows a global mean IAVA twice as large as the case in which $DIC_s{}'$ and T′ are also allowed to vary (compare in Figure 3b with 3a). The large increase in $\overline{pCO_2}$ and γ_{DIC} is similar for both groups of models and generates an overall amplification (Figure 4a,b). It is important to mention that the separation between $\overline{pCO_2}$ and γ_{DIC_s} is a mathematical construct rather than two separate phenomena. Ultimately, the change in $\overline{pCO_2} \cdot \gamma_{DIC_s}$ is what determines the increase in the DIC contribution, while the T contribution increases almost exclusively due to the increase in $\overline{pCO_2}$ since γ_T remains almost unchanged (not shown).

The damping of the pCO_2 IAVA (Figure 3 (a)) is due to a decrease of the DIC′ interannual variability. As shown in Figure 4 (c), the simulations differ in DIC′ creating a large spread in the projected IAVA (see Supplement Material Figure S9). The most striking difference between the groups of models is the location of the maximum DICs′ STD. In the first group of models, the maximum of the DIC′ standard deviation is located in the low latitudes, in contrast to Group II for which the maximum variability occurs in high latitudes.

Another important difference, is the future change on DIC IAV in the equatorial band. For Group I, the DIC STD largely decreases in this region, whereas for the models HadGEM2-CC/ES the STD increases. For the MPI-ESM-LR model, the STD slightly increases, but this model (as well as HadGEM2-CC/ES) is dominated by T in this region (see Figure 2). In high latitudes, for groups I and II the future DIC STD decreases but the sensitivity increases the most, resulting in a large amplification of pCO_2 variability. The high latitudes' strong sensitivity has been well documented in previous studies (Bates et al., 2014; Egleston et al., 2010; Fassbender et al., 2017). In summary, of the two groups of models, the Group II simulates a larger increase in the sensitivity and a smaller reduction on DIC′, therefore result in a larger pCO_2 IAVA than Group I. Interestingly, the T′ anomalies remain of similar magnitude during both periods of time, but as $[CO_2]$ increases, the overall T contribution is more amplified than the DIC contribution (see Supplement material, Figure S6).

The intra-model differences of future DIC′ and T′ IAV arise from the models' biophysical mechanisms, or due to possible future changes in the main modes of ocean-atmosphere variability, such as ENSO, NAO, SAM and PDO. An in-depth analysis of these causes is beyond the scope of this paper, but we discuss some possible explanations discussed in the current literature. One of the reasons for the diminished DIC′ variability may be related to the fact that models simulate a weaker Walker circulation in response to global warming (Vecchi et al., 2006; Zhao & Allen, 2019). A weaker Walker circulation would weaken the upwelling of DIC-rich waters during La Niña conditions.

Keller et al. (2015) studied ENSO variability in the CESM1-BGC model for the 850-2100 period, the authors found that the warmest period had the lowest variance in ENSO, and that the air-sea CO_2 flux response was the lowest. The latter result agrees with our finding that the pCO_2 variability decreases in the eastern equatorial Pacific for this model. However, unresolved large equatorial model biases with magnitude similar

©2020 American Geophysical Union. All rights reserved.

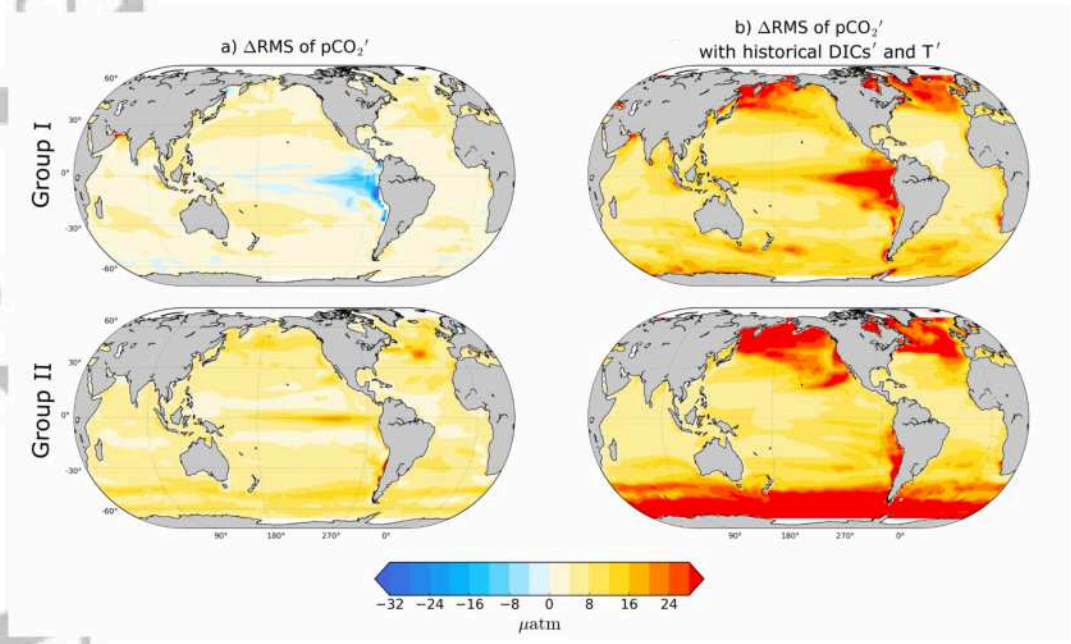

Figure 3. Causes of increasing sea surface pCO_2' variability: Total change (measured as 2045-2095 minus 1870-1920 values) of **a)** the RMS of pCO_2', **b)** RMS of pCO_2' when only the value of $\overline{pCO_2}$, γ_{DIC_s} and γ_T vary, but we keep the historical (1870-1920) value of the DIC_s' and T′ interannual anomalies. First we compute the total change for each model and subsequently take the ensemble mean of Group I (CanESM2, CESM1-BGC and GFDL-ESM2G) **(top row)** and Group II (HadGEM-CC/ES and MPI-ESM-LR) **(bottom row)**. Panel **b)** highlights that the RMS of pCO_2 increases due carbonate chemistry changes. However, the interannual variability of DIC and T generates differences between column a) and b) that depend on the models' physical and biological dynamics.

to the projected future warming (Cai et al., 2015; Timmermann et al., 2018) suggest that our model-based projections of future pCO_2 variability in the eastern equatorial could still be subject to larger uncertainties, which at this stage are difficult to quantify.

Another possible explanation for the diminished DIC′ variability is the projected shoaling of the winter mixed layer depth, associated with a reduced heat loss during the cold season. The mixed layer shoaling will cause less mixing of deep rich DIC waters to the surface on both, seasonal and interannual timescales. In the winter deep convection regions the future shoaling of the MLD may be underestimated by models, because they show a shallower than observed present-day mixed layer depth (Downes et al., 2009; Sallée et al., 2013). Simulations show that a decrease in mixed layer depth will also reduce the input of macronutrients and therefore reduce primary productivity (Bopp et al., 2013). However, in higher latitudes, such as the Southern Ocean, a reduction in light and temperature limitations estimulate primary productivity (Steinacher et al., 2010) which could counteract the decrease of the DIC′ variability.

The total reduction of the DIC′ STD may be a combination of these factors; for example, even if ENSO's magnitude and frequency increase, a reduction of the MLD may confine the ocean uptake of CO_2 to the surface, thereby reducing the DIC vertical gradient. As a result, frequent upwelling events would have a smaller impact on DIC′ IAV.

©2020 American Geophysical Union. All rights reserved.

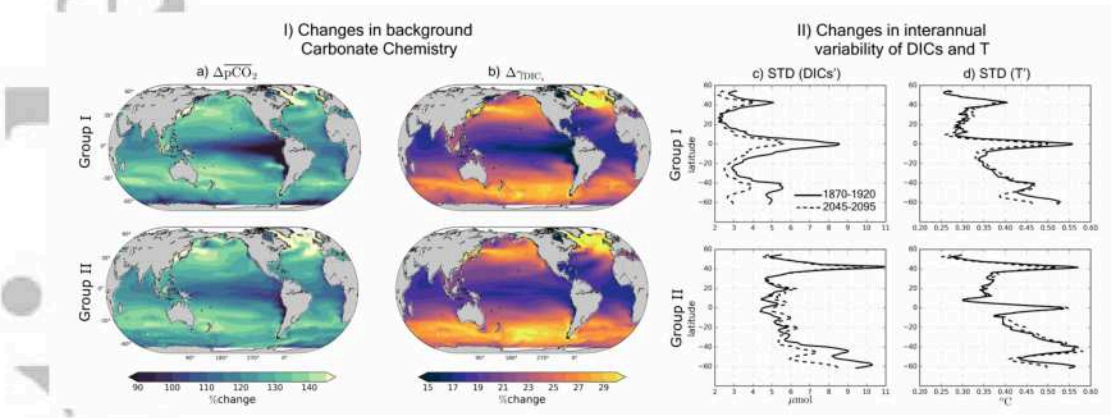

Figure 4. Changes in carbonate chemistry and interannual variability of surface DIC_s' and T'. Percentage change (measured as 2045-2095 minus 1870-1920 values) of **a)** $\overline{pCO_2}$ and **b)** γ_{DIC_s}. A 100% change indicates a doubling in magnitude. **c)** and **d)** show the ensemble mean of the zonally averaged standard deviation of DIC_s' and T' respectively. The **top** row shows the ensemble mean for models in Group I and the **bottom** for Group II.

4 Summary and Conclusions

The ocean surface pCO_2 responds to climate modes of variability that alter the ocean's circulation and biogeochemical conditions on interannual time-scales (Resplandy et al., 2015). The CMIP5 models present a larger present-day pCO_2 IAV than the observation-based estimates of Landschützer, Bushinsky, and Gray (2019). The difference can be partly attributed to the presence of near-annual variations that are less present in the Landschützer, Bushinsky, and Gray (2019) dataset, but that have a large impact on the dynamics of the simulated monthly anomalies of pCO_2.

Two opposing mechanisms control the simulated future changes in pCO_2 IAV. The first is the result of the changing ocean's carbonate chemistry; a higher background CO_2 concentration and increased oceanic sensitivity to anturally occurring DIC and T fluctuations amplify the pCO_2 IAV . The second opposing mechanism is a reduction of the interannual fluctuations in DIC that counteract the pCO_2 IAVA. In other words, although changes in DIC' will be smaller compared to present-day, the ocean will be much more sensitive to them and to T', resulting in an overall increase of pCO_2 variability in most of the global ocean. However, this result is based on fully-coupled ocean models with biases in mean state and variability. Beyond improving future earth system models in this regard, it is paramount to maintain extended carbonate chemistry observational networks that will help monitoring the interannual changes in DIC and pCO_2.

The response of the pCO_2 variability to greenhouse gases varies with latitude; most models show that the high latitudes with large pCO_2 IAV are also the ones that will be exposed to larger variance amplification, because the buffering capacity decreases faster in these regions (Egleston et al., 2010; Fassbender et al., 2017). The mid-latitudes variability will be mildly amplified by a larger pool of CO_2 that magnifies the response to T variability. In the equatorial Pacific the models show a larger discrepancy; the models that agree with present-day observations in terms of pCO_2 dynamics project a decrease in equatorial variability due to a large reduction of the DIC'. On the other hand, the HadGEM2-CC/ES and MPI-ESM-LR models show a small increase in equatorial variability, because their local pCO_2 IAV is dominated by T instead of DIC.

Accepted Article

©2020 American Geophysical Union. All rights reserved.

Accepted Article

Further study is required to detect how the pCO_2 IAVA will influence the regional and global CO_2 flux variability. Dong et al. (2016) found no increase in FCO_2 IAV in the CMIP5 models, however, the authors compared the STD of the FCO_2 anomalies between pre-industrial and present day levels, while we compared the end of the century levels with those at the onset of the industrial revolution. The increase in IAV is gradual and remains small at the beginning of the 21st. Therefore, longer time series are needed to detect the emerging forced amplification.

Changes of surface ocean pCO_2 on interannual time scales affect the source/sink nature of the ocean, and they may generate acidification and hypercapnia episodes on interannual time-scales in the most vulnerable regions (McNeil & Sasse, 2016; Sasse et al., 2015). In the mean time, future projections rely on ocean models as the current datasets are sparse and lack time continuity. The models' differences and similarities highlight the large gap in knowledge about the complex physical and biological factors modulated by ocean-atmosphere interactions that control the interannual variability, but also confirm the undeniable consequences of the changing background carbonate chemistry.

Acknowledgments

This work was supported by the National Science Foundation under Grant No. 1314209. A.T is supported by the Institute for Basic Science (IBS), South Korea under IBS-R028-D1. R.E.Z. acknowledges support from the US NSF (OCE15-58699). The CMIP5 data used in the analysis were obtained from https://esgf-node.llnl.gov/projects/esgf-llnl/ (last access: June 2019; Taylor et al. (2012)). The Landschützer, Bushinsky, and Gray (2019) pCO_2 data product is available at https://data.nodc.noaa.gov/cgi-bin/iso?id=gov.noaa.nodc:0191304 (last access: March 2020). The sea-surface temperature data corresponds to the National Oceanic and Atmospheric Administration's Optimum Interpolation version 234 SST product, which is available at https://www.esrl.noaa.gov/psd/data/gridded/data.noaa.oisst.v2.html.

References

Bakker, D. C. E., Pfeil, B., Landa, C. S., Metzl, N., O'Brien, K. M., Olsen, A., ... et al. (2016). A multi-decade record of high-quality fCO_2 data in version 3 of the Surface Ocean CO_2 Atlas (SOCAT). *Earth Syst. Sci. Data*, *8*, 383-413.

Bates, N. R., Astor, Y. M., Church, M. J., Currie, K., Dore, J. E., Gonzalez-Davila, M., ... Santana-Casiano, J. M. (2014). A Time-Series View of Changing Ocean Chemistry Due to Ocean Uptake of Anthropogenic CO_2 and Ocean Acidification. *Oceanopgraphy*, *27(1)*, 126-141.

Bopp, L., Resplandy, L., Orr, J. C., Doney, S. C., Dunne, J. P., Gehlen, M., ... Vichi, M. (2013). Multiple stressors of ocean ecosystems in the 21st century: projections with CMIP5 models. *Biogeosciences*, *10*, 6225–6245.

Cai, W., Santoso, A., Wang, G., Yeh, S., An, S., Cobb, K. M., & et al. (2015). ENSO and greenhouse warming. *Nature Climate Change*, *5*, 849-859.

Chatterjee, A., Gierach, M. M., Sutton, A. J., Feely, R. A., Crisp, D., Eldering, A., ... Schimel, D. S. (2017). Influence of El Niño on atmospheric CO_2 over the tropical Pacific Ocean: Findings from NASA's OCO-2 mission. *Science*, *358*(6360).

Cosca, C. E., Feely, R. A., Boutin, J., Etcheto, J., & McPhaden, M. J. (2003). Seasonal and interannual CO_2 fluxes for the central and eastern equatorial Pacific Ocean as determined from fCO_2-SST relationships. *J. Geophys. Res.*, *108(C8)*(3278).

Dickson, A. G. (1990). Thermodynamics of the dissociation of boric acid in synthetic seawater from 273.15 to 318.15 K. *Deep-Sea Research Part A. Oceanographic Research Papers*, *37*, 755–766.

Doney, S. C., Lima, I., Feely, R. A., Glover, D. M., Lindsay, K., Mahowald, N., ...

©2020 American Geophysical Union. All rights reserved.

Wanninkhof, R. (2009). Mechanisms governing interannual variability in upper-ocean inorganic carbon system and air–sea CO_2 fluxes: Physical climate and atmospheric dust. *Deep Sea Research Part II: Topical Studies in Oceanography*, *56*(8), 640 - 655. doi: https://doi.org/10.1016/j.dsr2.2008.12.006

Dong, F., Li, Y., & Wang, B. (2017). Assessment of responses of tropical Pacific air-sea CO_2 flux to ENSO in 14 CMIP5 models. *Journal of Climate*, *30*, 8595-8613.

Dong, F., Li, Y., Wang, B., Huang, W., Shi, Y., & Dong, W. (2016). Global Air-Sea CO_2 Flux in 22 CMIP5 Models: Multiyear Mean and Interannual Variability. *Journal of Climate*, *29*(7), 2407-2431.

Downes, S. M., Bindoff, N. L., & Rintoul, S. R. (2009). Impact of climate change on the subduction of mode and intermediate water masses in the Southern Ocean. *Journal of Climate*, *22*, 3289-3302.

Egleston, E. S., Sabine, C. L., & Morel, F. M. M. (2010). Revelle revisited: Buffer factors that quantify the response of ocean chemistry to changes in DIC and alkalinity. *Global Biogeochem. Cycles*, *24*, GB1002.

Fassbender, A. J., Rodgers, K. B., Palevsky, H. I., & Sabine, C. L. (2018). Seasonal asymmetry in the evolution of surface ocean pco_2 and ph thermodynamic drivers and the influence on sea-air co_2 flux. *Global Biogeochem. Cycles*, *32*.

Fassbender, A. J., Sabine, C. L., & Palevsky, H. I. (2017). Nonuniform ocean acidification and attenuation of the ocean carbon sink. *Geophysical Reserach Letters*, *44*, 8404–8413.

Feely, R. A., Boutin, J., Cosca, C. E., Dandonneau, Y., Etcheto, J., Inoue, H. Y., ... Wanninkhof, R. (2002). Seasonal and interannual variability of CO_2 in the equatorial Pacific. *Deep Sea Research Part II: Topical Studies in Oceanography*, *49*, 2443-2471.

Feely, R. A., Takahashi, T., Wanninkhof, R., McPhaden, M. J., Cosca, C. E., Sutherland, S. C., & Carr, M. E. (2006). Decadal variability of the air-sea CO_2 fluxes in the equatorial Pacific Ocean. *J. Geophys. Res.*, *111*(C08S90).

Feely, R. A., Wanninkhof, R., Takahashi, T., & Tans, P. (1999). Influence of El-Niño on the Equatorial Pacific contribution to atmospheric CO_2 accumulation. *Nature*, *398*, 597-601.

Friedrich, T., Oschlies, A., & Eden, C. (2006). Role of wind stress and heat fluxes in generating interannual-to-decadal variability of air-sea CO_2 and O_2 fluxes in a North Atlantic model. *Geophysical Reserach Letters*, *33*(LS21S04).

Gallego, M. A., Timmermann, A., Friedrich, T., & Zeebe, R. E. (2018). Drivers of future seasonal cycle changes in oceanic pCO_2. *Biogeosciences*, *15*, 5315-5327.

Gorgues, T., Aumont, O., & Rodgers, K. B. (2010). A mechanistic account of increasing seasonal variations in the rate of ocean uptake of anthropogenic carbon. *Biogeosciences*, *7*, 2581–2589.

Gregor, L., Kok, S., & Monteiro, P. M. S. (2018). Interannual drivers of the seasonal cycle of CO_2 in the Southern Ocean. *Biogeosciences*, *15*, 2361-2378.

Gruber, N., Landschützer, P., & Lovenduski, N. S. (2019). The variable southern ocean carbon sink. *Annu. Rev. Mar. Sci.*, *11*, 16.1-16.28.

Hauck, J., & Völker, C. (2015). Rising atmospheric CO_2 leads to large impact of biology on Southern Ocean CO_2 uptake via changes of the Revelle factor. *Geophysical Reserach Letters*, *42*, 1459–1464.

Hauri, C., Friedrich, T., & Timmermann, A. (2015). Abrupt onset and prolongation of aragonite undersaturation events in the Southern Ocean. *Nat. Clim. Change*, *6*, 172–176.

IPCC. (2013). *IPCC Climate Change 2013: The Physical Science Basis. Contribution of Working Group i to the Fifth Assessment Report of the Intergovernmental Panel on Climate Change*. Cambridge, United Kingdom and New York, NY, USA: Cambridge University Press.

Jin, C., Zhou, T., & Chen, X. (2019). Can CIMP5 Earth System Models repro-

©2020 American Geophysical Union. All rights reserved.

duce the interannual variability of air-sea CO_2 fluxes over the tropical Pacific Ocean? *J. Climate*, *32*, 2261-2275.

Keller, K. M., Joos, F., Lehner, F., & Raible, C. C. (2015). Detecting changes in marine responses to ENSO from 850 to 2100 C.E.: Insights from the ocean carbon cycle. *Geophysical Reserach Letters*, *42*.

Kwiatkowski, L., & Orr, J. (2018). Diverging seasonal extremes for ocean acidification during the twenty-first century. *Nat. Clim. Change*, *8*, 141–145.

Landschützer, P., Bushinsky, S. M., & Gray, A. R. (2019). A combined globally mapped carbon dioxide (co_2) flux estimate based on the surface ocean co_2 atlas database (socat) and southern ocean carbon and climate observations and modeling (soccom) biogeochemistry floats from 1982 to 2017 (ncei accession 0191304). *NOAA National Centers for Environmental Information.*

Landschützer, P., Gruber, N., & Bakker, D. (2017). *An updated observation-based global monthly gridded sea surface pCO_2 and air-sea CO_2 flux product from 1982 through 2015 and its monthly climatology (NCEI Accession 0160558). Version 2.2. NOAA National Centers for Environmental Information. Dataset. doi:10.7289/v5z899n6.*

Landschützer, P., Gruber, N., & Bakker, D. C. E. (2016). Decadal variations and trends of the global carbon sink. *Global Biogeochem. Cycles*, *30*, 1396-1417.

Landschützer, P., Gruber, N., Bakker, D. C. E., Stemmler, I., & Six, K. D. (2018). Strengthening seasonal marine CO_2 variations due to increasing atmospheric CO_2. *Nat. Clim. Change*, *8*, 146–150.

Landschützer, P., Ilyina, T., & Lovenduski, N. (2019). Detecting regional modes of variability in observation-based surface ocean pCO_2. *Geophysical Reserach Letters*, *46*, 2670-2679.

Le Quéré, C., Andrew, R. M., Friedlingstein, P., Sitch, S., Hauck, J., Pongratz, J., et al. (2018). Global carbon budget 2018. *Earth Syst. Sci. Data Discuss*(1-3).

Le Quéré, C., Orr, J. C., Monfray, P., & Aumont, O. (2000). Interannual variability of the oceanic sink of CO_2 from 1979 through 1997. *Global Biogeochem. Cycles*, *14*(4), 1247-1265.

Li, H., Ilyina, T., Müller, W. A., & Landschützer, P. (2019). Predicting the variable ocean carbon sink. *Science Advances*, *5*(eaav6471).

Long, M., Lindsay, K., Peacock, S., Moore, J. K., & Doney, S. C. (2013). Twentieth-century oceanic carbon uptake and storage in CESM1(BGC). *J. Climate*, *26*, 6775-6800.

Lovenduski, N. S., Gruber, N., Doney, S. C., & Lima, I. D. (2007). Enhanced CO_2 outgassing in the Southern Ocean from a positive phase of the Southern Annular Mode. *Global Biogeochem. Cycles*, *21*, GB2026.

McKinley, G. A., Fay, A. R., Lovenduski, N. S., & Pilcher, D. J. (2017). Natural variability and anthropogenic trends in the ocean carbon sink. *Annu. Rev. Mar. Sci.*, *9*, 9.1-9.26.

McKinley, G. A., Follows, M. J., & Marshall, J. (2004). Mechanisms of air-sea CO_2 flux variability in the equatorial Pacific and the North Atlantic. *Global Biogeochem. Cycles*, *18*(GB2011).

McNeil, B. I., & Sasse, T. P. (2016). Future ocean hypercapnia driven by anthropogenic amplification of the natural CO_2 cycle. *Nature*, *529*, 383–386.

Millero, F. J. (1995). Thermodynamics of the carbon dioxide system in the oceans. *Geochemica et Cosmochemica Acta*, *59*, 661–677.

Millero, F. J., Graham, T. B., Huang, F., Bustos-Serrano, H., & Pierrot, D. (2006). Dissociation constants of carbonic acid in seawater as a function of salinity and temperature. *Marine Chemistry*, *100(1–2)*, 80–94.

Park, G. H., Wanninkhof, R., Doney, S. C., Takahashi, T., Lee, K., Feely, R. A., ... Triñanes, J. (2010). Variability of global net sea–air CO_2 fluxes over the last three decades using empirical relationships. *Tellus B*, *62B*, 352-368.

Resplandy, L. R., Séférian, R., & Bopp, L. (2015). Natural variability of CO_2: What

©2020 American Geophysical Union. All rights reserved.

can we learn from centuries-long climate models simulations? *J. Geophys. Res. Oceans*, *120*, 384-404.

Rödenbeck, C., Bakker, D., Metzl, N., Olsen, A., Sabine, C., Cassar, N., ... Heimann, M. (2014). Interannual sea–air CO_2 flux variability from an observation-driven ocean mixed-layer scheme. *Biogeosciences*, *11*, 4599-4613.

Rödenbeck, C., Bakker, D. C. E., Gruber, N., Iida, Y., Jacobson, A. R., Jones, S., ... Zeng, J. (2015). Data-based estimates of the ocean carbon sink variability – first results of the Surface Ocean pCO_2 Mapping intercomparison (SOCOM). *Biogeosciences*, *12*, 7251-7278.

Sabine, C. L., Feely, R. A., Gruber, N., Key, R. M., Lee, K., Bullister, J. L., ... Rios, A. F. (2004). The oceanic sink for anthropogenic CO_2. *Science*, *305*, 367–371.

Sabine, C. L., Hankin, S., Koyuk, H., Bakker, D. C. E., Pfeil, B., Olsen, A., ... others (2013). Surface Ocean CO_2 Atlas (SOCAT) gridded data products. *Earth Syst. Sci. Data*, *5*, 145-153.

Sallée, J. B., Shuckburgh, E., Bruneau, N., Meijers, A. J. S., Bracegirdle, T. J., & Wang, Z. (2013). Assessment of Southern Ocean mixed-layer depths in CMIP5 models: Historical bias and forcing response. *Geophysical Research Oceans*, *118*, 1845-1862.

Sasse, T., McNeil, B. I., Matear, R., & Lenton, A. (2015). Quantifying the influence of CO_2 seasonality on future aragonite undersaturation onset. *Biogeosciences*, *12*, 6017-6031.

Séférian, R., Berthet, S., & Chevallier, M. (2018). Assessing the decadal predictability of land and ocean carbon uptake. *Geophysical Reserach Letters*, *45*, 2455-2466.

Steinacher, M., Joos, F., Froelicher, T. L., Bopp, L., Cadule, P., Cocco, V., ... Segschneider, J. (2010). Projected 21st century decrease in marine productivity: a multi-model analysis. *Biogeosciences*, *7*, 979–1005.

Stuecker, M. F., Jin, F., Timmermann, A., & McGregor, S. (2015). Combination mode dynamics of the anomalous northwest Pacific anticyclone. *Journal of Climate*, *28*, 1093-1111.

Sutton, A. J., Feely, R. A., Sabine, C. L., McPhaden, M. J., Takahashi, T., Chavez, F. P., ... Mathis, J. T. (2014). Natural variability and anthropogenic change in equatorial Pacific surface ocean pCO_2 and pH. *Global Biogeochem. Cycles*, *28*, 131-145.

Sutton, A. J., Wanninkhof, R., Sabine, C. L., Feely, R. A., Cronin, M. F., & Weller, R. A. (2017). Variability and trends in surface seawater pCO_2 and CO_2 flux in the Pacific Ocean. *Geophysical Reserach Letters*, *44*, 5627-5636.

Takahashi, T., Olafsson, J., Goddard, J. G., Chipman, D. W., & Sutherland, S. C. (1993). Seasonal variation of CO_2 and nutrients in the high-latitude surface oceans: A comparative study. *Global Biogeochem. Cycles*, *7*, 843–878.

Takahashi, T., Sutherland, S. C., Sweeney, C., Poisson, A., Metzl, N., Tilbrook, B., ... Nojiri, Y. (2002). Global sea-air CO_2 flux based on climatological surface ocean pCO_2, and seasonal biological and temperature effects. *Deep-Sea Research II*, *49*, 1601–1623.

Taylor, K. E., Stouffer, R. J., & Meehl, G. A. (2012). An Overview of CMIP5 and the experiment design, B. *Am. Meteorol. Soc.*, *93*, 485-489.

Timmermann, A., An, S., Kug, J., Jin, F., Cai, W., Capotondi, A., ... et al. (2018). El Niño–Southern Oscillation complexity. *Nature*, *559*(7715), 535-543.

Tjiputra, J. F., Olsen, A. R. E., Bopp, L., Lenton, A., Pfeil, B., Roy, T., ... Heinze, C. (2014). Long-term surface pCO_2 trends from observations and models. *Tellus B*, *66*(23083).

Valsala, V. K., Roxy, M. K., Ashok, K., & Murtugudde, R. (2014). Spatiotemporal characteristics of seasonal to multidecadal variability of pCO_2 and air-sea CO_2 fluxes in the equatorial Pacific Ocean. *J. Geophys. Res. Oceans*, *119*,

Accepted Article

©2020 American Geophysical Union. All rights reserved.

8987–9012.

Vecchi, G. A., Soden, B. J., Wittenberg, A. T., Held, I. M., & Leetmaa, A. (2006). Weakening of tropical Pacific atmospheric circulation due to anthropogenic forcing. *Nature*, *441*, 73-76.

Verdy, A., Dutkiewicz, S., Follows, M. J., Marshall, J., & Czaja, A. (2007). Carbon dioxide and oxygen fluxes in the Southern Ocean: Mechanisms of interannual variability. *Global Biogeochem. Cycles*, *21*(GB2020).

Wang, X., Murtugudde, R., Hackert, E., Wang, J., & Beauchamp, J. (2015). Seasonal to decadal variations of sea surface pCO_2 and sea-air CO_2 flux in the equatorial oceans over 1984–2013: A basin-scale comparison of the Pacific and Atlantic Oceans. *Global Biogeochem. Cycles*.

Wanninkhof, R., & Triñanes, J. (2017). The impact of changing wind speeds on gas transfer and its effect on global air-sea co_2 fluxes. *Global Biogeochem. Cycles*, *31*, 961-974.

Zeebe, R. E., & Wolf-Gladrow, D. (2001). *CO_2 in Seawater: Equilibrium, Kinetics, Isotopes.* Amsterdam, Netherlands, and Philadelphia, PA, USA: Elsevier Science.

Zhao, X., & Allen, R. J. (2019). Strengthening of the Walker Circulation in recent decades and the role of natural sea surface temperature variability. *Environ. Res. Commun*, *1*(021003).

Accepted Article

©2020 American Geophysical Union. All rights reserved.